

Constraining the anisotropy of the Universe with the X-ray and UV fluxes of quasars

Dong Zhao, Jun-Qing Xia^a

Department of Astronomy, Beijing Normal University, Beijing 100875, China

Received: date / Revised version: date

Abstract We test the anisotropy in the Finslerian cosmological model with the X-ray and ultraviolet (UV) fluxes of 808 quasars. The dipole amplitude is $A_D = 0.302^{+0.185}_{-0.124}$ and the dipole direction points towards $(l, b) = (288.92^{+23.74^\circ}_{-28.80^\circ}, 6.10^{+16.55^\circ}_{-16.40^\circ})$. We find that the dipole direction from the X-ray and UV fluxes of quasars is very close to the dipole direction given by the “Joint Light-curve Analysis” (JLA) compilation in the Finslerian cosmological model and the angular difference between the two dipole directions is only 10.44° . We also find the angular difference between the dipole direction from the 808 quasars in the Finslerian cosmological model and ones from the supernovae of type Ia (SNe Ia) samples in the dipole-modulated Λ CDM model is around 30° . Six gravitationally lensed quasars are considered to investigate the Hubble constant H_0 in the Finslerian cosmological model. We get a slightly smaller H_0 than the result given by the six gravitationally lensed quasars. Finally, we forecast the future constraints on the dipole parameters with the X-ray and UV fluxes of quasars. As the number of simulations increases, the precisions of the parameters related to anisotropy in the Finslerian cosmological model improve significantly. The X-ray and UV fluxes of quasars have a promising future as a probe of anisotropy in Finsler spacetime.

PACS. 98.80.k cosmology – 98.65.Dx large-scale structure of the Universe

1 Introduction

The Universe is homogeneous and isotropic on large scale, which is called the cosmological principle. Based on it, the standard Lambda cold dark matter (Λ CDM) cosmological model has been established. In the past few decades, many experiments test its validity and verify that it is consistent with most cosmological observations. The observations of Cosmic Microwave Background (CMB) temperature anisotropies and polarizations from Wilkinson Microwave Anisotropy Probe (WMAP) [1, 2] and Planck satellites [3–6] provide high-precision constraints on the six based cosmological parameters. However, there still exist several anomalies that have been reported, such as the alignment of low- ℓ multipoles in the CMB temperature anisotropies [7–10], the parity asymmetry [6, 11–15] and the hemispherical power asymmetry [6, 16–18] in CMB, the spatial variation of the fine structure constant [19, 20], the anisotropic accelerating expansion of the Universe [21–26], the alignment of quasar polarization vectors on large scale [27], the MOND acceleration scale [28–30]. These phenomena may imply that our Universe has a preferred direction.

As the most luminous and persistent energy source, quasars have extraordinary potential in the exploration of our Universe. In recent years, quasars are tentatively

used to investigate the cosmological parameters. An incomplete list includes the relation between the UV emission lines and the continuum luminosity [31], the relation between the radius of quasars and its luminosity [32–34], the relation between luminosity and mass of super Eddington accreting quasars [35], the correlation between X-ray variability and luminosity of quasars [36], the non-linear relation between UV and X-ray luminosity [37–40]. The non-linear relation between UV and X-ray luminosity was firstly discovered by the X-ray surveys [41–43]. For decades, the UV and X-ray luminosity relationship has been confirmed by observations of a few hundred quasars in the redshift range from 0 to 6.5. Since 2015, E. Lusso etc. [37, 40] have been attempting to estimate the cosmological parameters by the non-linear relation between UV and X-ray luminosity with quasars as standardizable candles.

In this paper, we will use the X-ray and UV fluxes of 808 quasars [37] to explore the anisotropy in the Universe. These 808 quasars are thought to be standardizable candles through the relation between UV and X-ray luminosity. The quasars sample is in the redshift range $0.061 \leq z \leq 6.28$. The Pantheon sample [44] and the JLA compilation [45] are combined with 808 quasars in the analysis of the anisotropic cosmological model i.e., Finslerian cosmological model. We also attempt to investigate the Hubble constant H_0 in the Finslerian cos-

^a xiajq@bnu.edu.cn

mological model by considering six gravitationally lensed quasars with measured time delays [46]. At last, we will forecast the future constraints on the Finslerian cosmological model with the X-ray and UV fluxes of quasars.

The rest of this paper is organized as follows. In Section 2, we briefly introduce the UV and X-ray luminosity relationship, the Time-Delay Strong Lensing measurement, and the Finslerian cosmological model. We show our results in Section 3. Finally, discussions and conclusions are given in Section 4.

2 Methodology

2.1 The UV and X-ray luminosity relationship

The relation of the UV and X-ray luminosity is parameterized as

$$\alpha_{\text{OX}} = 0.384 \times \log(L_X/L_{\text{UV}}), \quad (1)$$

where L_{UV} denotes the logarithm of the monochromatic luminosity at 2500 Å and L_X denotes the logarithm of the monochromatic luminosity at 2 keV. α_{OX} is the slope of power law, which connects L_X and L_{UV} . Eq. (1) can be written as

$$\log L_X = \beta + \gamma \log L_{\text{UV}}, \quad (2)$$

where β and γ are two free parameters. The luminosities and fluxes of quasars are connected by the luminosity distance. Now we rewrite the Eq. (2) and obtain

$$\log(F_X) = \beta + (\gamma - 1) \log(4\pi) + \gamma \log(F_{\text{UV}}) + 2(\gamma - 1) \log(D_L), \quad (3)$$

where \log denotes \log_{10} . F_X and F_{UV} represent the X-ray and UV fluxes of quasars, respectively. The luminosity distance D_L takes the form,

$$D_L = \frac{c(1+z)}{H_0} \int_0^z \frac{dz'}{E(z')}, \quad (4)$$

where z_{cmb} denotes redshift. c is the speed of light and H_0 is the Hubble constant. The expression of $E(z)$ depends on cosmological models.

In our work, the dataset of the X-ray and UV fluxes of quasars are from G. Risaliti and E. Lusso [37]. The dataset contains 808 quasars, which are in the redshift range $0.061 \leq z \leq 6.28$. The redshift distribution of 808 quasars is shown in Fig. 1. The distribution of 808 quasars in the galactic coordinate system is shown in Fig. 2 and the pseudo-colors indicate the redshift of these quasars.

2.2 The Time-Delay Strong Lensing measurement

Strong gravitational lensing is a powerful probe of cosmological models. The time-delay strong lensing (TDSL) measurement is a fully independent method to measure the Hubble constant. Since the approach first proposed by Refsdal [47], lensed quasars have generally been used to constrain H_0 by measuring the difference in arrival time

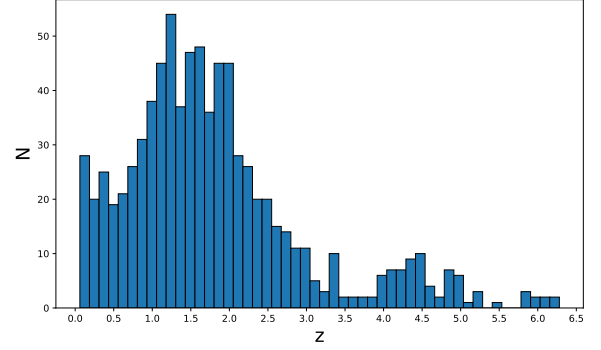


Figure 1. The redshift distribution of 808 quasars.

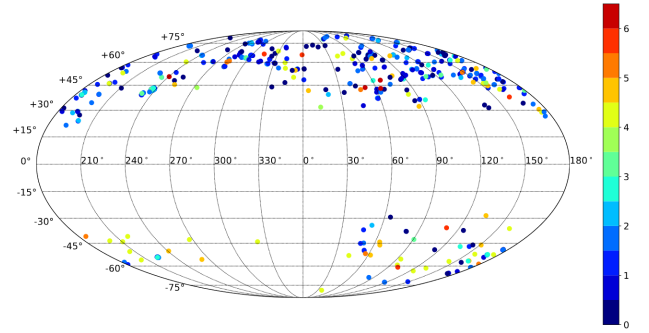


Figure 2. The distribution of 808 quasars in the galactic coordinate system. The pseudo-colors indicate redshift of these quasars.

of photons. TDSL provides a measurement of H_0 , which is completely independent of the CMB and the local distance ladder.

The travel time of light rays from a source to the observer depends on their path length and the gravitational potential they traverse. For a system of lenses with an image at an angular position θ and corresponding source position β , the excess time delay is

$$t(\theta, \beta) = \frac{D_{\Delta t}}{c} \left[\frac{(\theta - \beta)^2}{2} - \psi(\theta) \right], \quad (5)$$

where c is the speed of light and $\psi(\theta)$ is the lens potential. The time-delay distance $D_{\Delta t}$ is defined as [47]

$$D_{\Delta t} = (1 + z_d) \frac{D_d D_s}{D_{\text{ds}}}, \quad (6)$$

where z_d denotes the lens redshift. D_d and D_s are the angular diameter distance from the observer to the lens and the angular diameter distance from the observer to the source, respectively. D_{ds} is the angular diameter distance from the lens to the source. The angular diameter distance is defined as

$$D_A = \frac{c}{H_0(1+z)} \int_0^z \frac{dz'}{E(z')}, \quad (7)$$

where z is the redshift and H_0 is the Hubble constant. The expression of $E(z)$ depends on cosmological models. The difference of excess time delays between two images A and B is

$$\Delta t_{AB} = \frac{D_{\Delta t}}{c} \left[\frac{(\theta_A - \beta)^2}{2} - \psi(\theta_A) - \frac{(\theta_B - \beta)^2}{2} + \psi(\theta_B) \right], \quad (8)$$

where θ_A and θ_B are the positions of image A and B, respectively.

We use six gravitationally lensed quasars with measured time delays from H0LiCOW collaboration [46] to constrain the Hubble constant and other cosmological parameters. Our work is based on the H_0 inference code¹ provided by Kenneth C. Wong etc. [46].

2.3 The anisotropic cosmological model

In this paper, we choose the Finslerian cosmological model as the anisotropic cosmological model. Different from the standard cosmological model, the Finslerian cosmological model has an intrinsically preferred direction that breaks the isotropy of the Universe. Many works about investigating the anisotropy of the Universe are based on the Finsler spacetime. For instance, investigating the cosmic anisotropy with supernovae of type Ia (SNe Ia) samples by the hemisphere comparison HC method [25, 48] and the dipole fitting [25, 26, 49–51], explaining the parity asymmetry and power deficit in the Finsler spacetime [52], the unified description for dipoles of the fine-structure constant and SNe Ia Hubble diagram [53].

In the Finsler spacetime, the scale factor a takes the form [53],

$$a = (1 + A_D \cos \theta) / (1 + z). \quad (9)$$

A_D is a parameter in the Finsler spacetime, which can be regarded as the dipole amplitude. When $A_D = 0$, the Finslerian cosmological model reduces to the Λ CDM model. $\cos \theta$ is the angle between the position of quasars and the preferred direction in the Finsler spacetime. By Eq. (9), the luminosity distance in the Finsler spacetime can be written as

$$D_L = \frac{c(1+z)}{H_0} \int_0^z \frac{dz'}{E(z')}, \quad (10)$$

where $E(z)$ in the Finsler spacetime takes the form of

$$E(z) = \sqrt{\Omega_{m0}(1+z)^3(1+A_D \cos \theta)^{-3} + 1 - \Omega_{m0}}. \quad (11)$$

Plugging Eq. (11) into Eq. (4) and Eq. (7), we can get the form of the luminosity distance and angular diameter distance in the Finslerian cosmological model, respectively.

3 Results

To constrain the dipole amplitude and the preferred direction in the Finslerian cosmological model with the

X-ray and UV fluxes of quasars, we employ the likelihood function [38],

$$\ln(\text{LF}) = -\frac{1}{2} \sum_{i=1}^N \left[\frac{[\log(F_{X,i}^{\text{obs}}) - \log(F_{X,i}^{\text{th}})]^2}{s_i^2} + \ln(2\pi s_i^2) \right], \quad (12)$$

where $s_i^2 = \sigma_i^2 + \delta^2$. σ_i^2 is the error of the observed flux $F_{X,i}^{\text{obs}}$ and δ is the global intrinsic dispersion. $F_{X,i}^{\text{th}}$ is the theoretical flux at the redshift z_i .

The Markov chain Monte Carlo (MCMC) method has been used to explore the whole parameters space in our work. Emcee² [54] as the Affine Invariant Markov chain Monte Carlo Ensemble sampler is widely used to investigate the parameters in astrophysics and cosmology. During the fitting process, we find that the parameters β , γ , and δ are insensitive to the Λ CDM model and the Finslerian cosmological model. The results of the three parameters in the two cosmological models are almost the same. For the sake of brevity and clarity, we only show the parameters related to the Finslerian cosmological model.

The flat prior of each parameter in the Finslerian cosmological model is

$$\Omega_m \sim [0, 1], A_D \sim [0, 1], l \sim [-180, 180], b \sim [-90, 90]. \quad (13)$$

The results are shown in Fig. 3 and summarized in Table 1. In Fig. 3, we show the marginalized posterior distribution of the parameters. The horizontal and vertical solid black lines denote the maximum of 1-dimensional marginalized posteriors. In Table 1, we show the 68% confidence level constraints on the parameters. As can be seen, the dipole anisotropy is well-constrained by the X-ray and UV fluxes of quasars. The dipole amplitude is $A_D = 0.302_{-0.124}^{+0.185}$, which is not zero in 1σ confidence level. The dipole direction points towards $(l, b) = (288.92_{-28.80}^{+23.74}, 6.10_{-16.40}^{+16.55})$. Compared with results from SNe Ia [48, 50, 51], the precision of dipole direction has a significant improvement. Interestingly, we found that the dipole direction from the X-ray and UV fluxes of quasars is very close to the dipole direction $(l, b) = (291.60_{-92.96}^{+248.10}, 16.20_{-78.73}^{+73.80})$ given by the JLA in the Finslerian cosmological model. The angular difference between the two dipole directions is only 10.44° . The dipole direction given by the Pantheon sample in the Finslerian cosmological model is $(l, b) = (298.80_{-118.69}^{+75.31}, -23.41_{-57.41}^{+19.26})$ [51], which is about 31.05° away from the dipole direction given by the X-ray and UV fluxes of quasars.

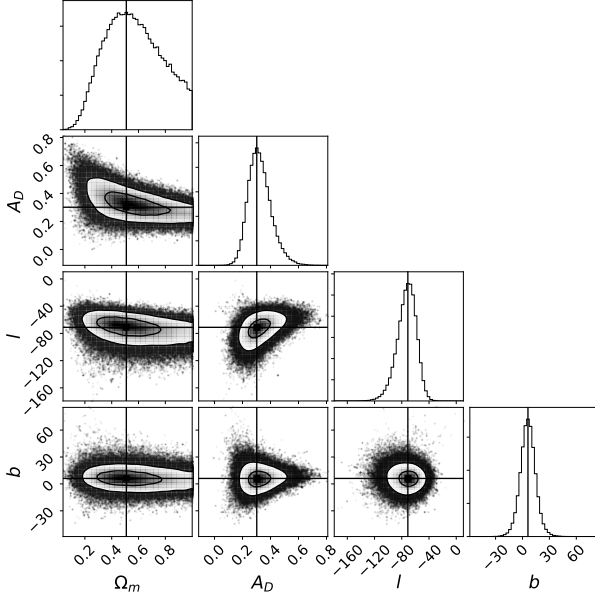
The dipole directions from SNe Ia in the dipole-modulated Λ CDM model are also considered for comparison. In Table 2, we summarized the dipole directions in the dipole-modulated Λ CDM model. In Fig. 4, we show all the dipole directions mentioned above in the galactic coordinate system. As can be seen in Fig. 4, the dipole direction given by the X-ray and UV fluxes of quasars is not far away from the dipole directions given by SNe Ia in the dipole-modulated Λ CDM model. We show the angular difference between the dipole direction given by the X-ray and UV

¹ https://github.com/shsuyu/H0LiCOW-public/tree/master/H0_inference_code.

² <https://emcee.readthedocs.io/en/stable/>

Table 1. The 68% confidence level constraints on the parameters in the Finslerian cosmological model with different datasets.

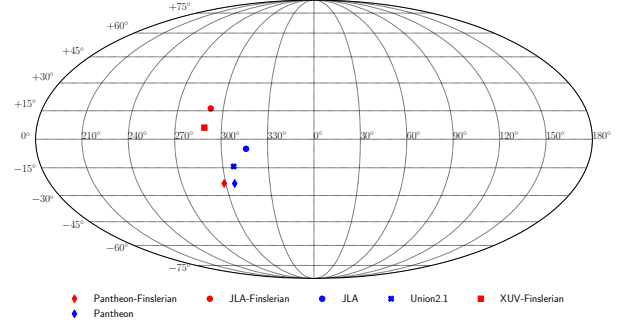
Data	Quasars	Quasars + Pantheon + JLA	Quasars + TSDL
Ω_m	$0.509^{+0.453}_{-0.275}$	$0.298^{+0.039}_{-0.042}$	$0.204^{+0.190}_{-0.137}$
A_D	$0.302^{+0.185}_{-0.124}$	—	$0.142^{+0.330}_{-0.142}$
l	$288.92^{+23.74}_{-28.80}$	$284.41^{+220.14}_{-104.37}$	$296.24^{+46.62}_{-94.22}$
b	$6.10^{+16.55}_{-16.40}$	$-9.00^{+76.29}_{-80.99}$	$21.23^{+51.33}_{-45.86}$
H_0^1	—	—	$72.2^{+3.6}_{-4.1}$

¹ km s⁻¹Mpc⁻¹**Figure 3.** The marginalized posterior distribution of the parameters in the Finslerian cosmological model with the X-ray and UV fluxes of quasars. The horizontal and vertical solid black lines denote the maximum of 1-dimensional marginalized posteriors.**Table 2.** The 68% confidence level constraints on the dipole directions in the dipole-modulated Λ CDM model with Pantheon [48], JLA [50], and Union2.1 [55].

Data	Pantheon	JLA	Union2.1
l	$306.00^{+82.95}_{-125.01}$	316^{+107}_{-110}	$307.1^\circ \pm 16.2^\circ$
b	$-34.20^{+16.82}_{-54.93}$	-5^{+41}_{-60}	$-14.3^\circ \pm 10.1^\circ$

fluxes of quasars and other dipole directions in Table 3. For the three dipole directions in the dipole-modulated Λ CDM model, the angular difference is around 30°. The dipole direction from the X-ray and UV fluxes of quasars close to the ones from the SNe Ia sample, especially the JLA compilation, may hint that there could exist an underlying relation.

We combined the Pantheon sample and JLA compilation with quasars to constrain the Finslerian cosmological model. The results are shown in Fig. 5 and summarized in Table 1. In Fig. 5, we show the marginalized posterior distribution of the parameters. The hor-

**Figure 4.** The dipole directions from the Finslerian cosmological model and the dipole-modulated Λ CDM model with different datasets in the galactic coordinate system.

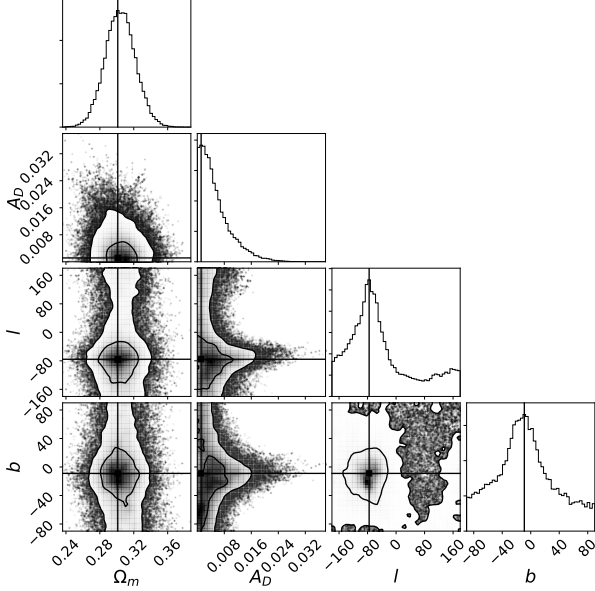
izontal and vertical solid black lines denote the maximum of 1-dimensional marginalized posteriors. In Table 1, we show the 68% confidence level constraints on the parameters. For the combined datasets, the 95% confidence level upper limit of the dipole amplitude A_D is 1.14×10^{-2} and the dipole direction points towards $(l, b) = (284.41^{+220.14}_{-104.37}, -9.00^{+76.29}_{-80.99})$. The result is similar to one from the Pantheon sample in the Finslerian cosmological model [51].

To investigate the Hubble constant H_0 in the Finslerian cosmological model, we use six gravitationally lensed quasars with measured time delays from H0LiCOW collaboration [46] in our analysis. The six gravitationally lensed quasars are combined with the X-ray and UV fluxes of quasars in the parameters fitting. The flat prior on each parameter is as follow: $H_0 \sim [60, 100]$, $\Omega_m \sim [0, 1]$, $A_D \sim [0, 1]$, $l \sim [-180, 180]$, $b \sim [-90, 90]$. We show the results in Fig. 6 and Table 1. We find that the dipole amplitude is $A_D = 0.142^{+0.330}_{-0.142}$ and the dipole direction is $(l, b) = (296.24^{+46.62}_{-94.22}, 21.23^{+51.33}_{-45.86})$. Even though the errors of parameters are bigger than ones given by quasars, the results of parameters related to anisotropy are consistent with the results from quasars. The Hubble constant is $H_0 = 72.2^{+3.6}_{-4.1}$ km s⁻¹Mpc⁻¹. Compared with the results from six gravitationally lensed quasars with measured time delays $H_0 = 73.3^{+1.7}_{-1.8}$ km s⁻¹Mpc⁻¹ [46], the central value of H_0 decreases a little bit.

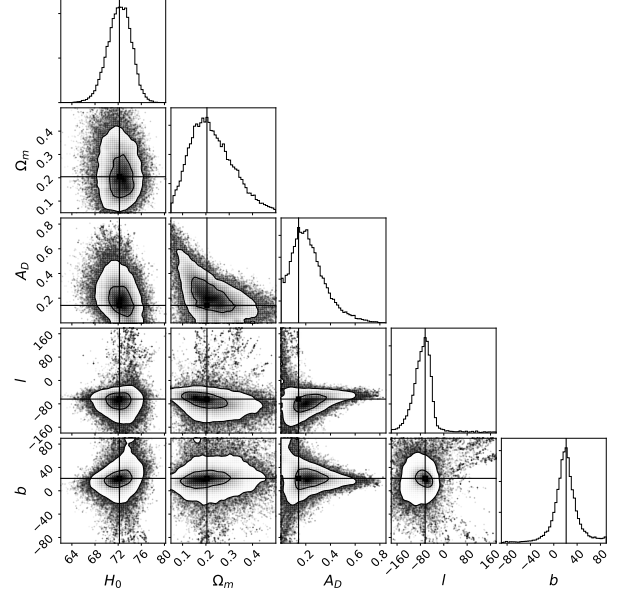
Finally, we forecast the future constraints on the dipole parameters in the Finslerian cosmological model with the X-ray and UV fluxes of quasars. We assume Finslerian cosmological model with $\Omega_m = 0.509$, $A_D = 0.302$ and

Table 3. The angular difference between the dipole direction given by the X-ray and UV fluxes of quasars and other dipole directions. “F” denotes the Finslerian cosmological model and “ Λ ” denotes the Λ CDM model.

Dipole direction	Pantheon-F	JLA-F	Pantheon- Λ	JLA- Λ	Union2.1- Λ
Difference	31.05°	10.44°	33.90°	29.23°	27.23°

**Figure 5.** The marginalized posterior distribution of the parameters in the Finslerian cosmological model from quasars, Pantheon sample, and JLA compilation. The horizontal and vertical solid black lines denote the maximum of 1-dimensional marginalized posteriors.

$(l, b) = (288.92^\circ, 6.10^\circ)$, which are given by the the X-ray and UV fluxes of 808 quasars. In the simulation, the positions of the 808 quasars are unchanged and the redshifts of simulated quasars are generated from the redshift distribution of the 808 quasars. We replace the X-ray fluxes of i th simulated quasar with a random number generated from the Gaussian distribution $G(F_X^{\text{obs}}, \sigma_{F_X^{\text{obs}}})$, where the F_X^{obs} is the X-ray fluxes of observed quasars at the same position with the i th simulated quasar and $\sigma_{F_X^{\text{obs}}}$ is the error of the observed flux $F_{X,i}^{\text{obs}}$. We construct 2000, 5000, and 10000 simulations for comparison, and the results of the dipole parameters from the simulated dataset are shown in Fig. 7 and summarized in Table 4. In Fig. 7, the blue, red, and dark lines denote 2000, 5000, and 10000 simulations, respectively. As can be seen, the inferred errors of the dipole parameters get smaller as the number of simulations increases. For the dipole amplitude A_D , the inferred error of lower and upper limits reduce to 12.76% and 15.86%. For the direction parameters l and b , the precisions increase by about 50% when the 2000 simulations are compared with the 10000 simulations. Our results show that the X-ray and UV fluxes of quasars have a promising future as a probe of the Finslerian cosmological model.

**Figure 6.** The marginalized posterior distribution of the parameters related to the Finslerian cosmological model with six gravitationally lensed quasars and the X-ray and UV fluxes of quasars. The horizontal and vertical solid black lines denote the maximum of 1-dimensional marginalized posteriors.**Table 4.** The 68% confidence level constraints on the parameters in the Finslerian cosmological model with the simulated dataset.

Simulations	2000	5000	10000
A_D	$0.280^{+0.105}_{-0.078}$	$0.289^{+0.065}_{-0.054}$	$0.290^{+0.046}_{-0.037}$
l	$288.35^{+16.15^\circ}_{-19.92^\circ}$	$289.70^{+9.81^\circ}_{-11.78^\circ}$	$289.00^{+7.73^\circ}_{-7.57^\circ}$
b	$6.66^{+11.45^\circ}_{-12.17^\circ}$	$5.81^{+7.36^\circ}_{-6.47^\circ}$	$6.40^{+4.64^\circ}_{-4.87^\circ}$

4 Discussions and conclusions

In this paper, we tested the anisotropy in the Finslerian cosmological model with the X-ray and UV fluxes of quasars. The dipole anisotropy is well-constrained by the X-ray and UV fluxes of quasars. The dipole amplitude is $A_D = 0.302^{+0.185}_{-0.124}$ and the dipole direction points towards $(l, b) = (288.92^\circ \pm 23.74^\circ, 6.10^\circ \pm 16.55^\circ)$. Interestingly, we found that the dipole direction from the X-ray and UV fluxes of quasars is very close to the dipole direction $(l, b) = (291.60^\circ \pm 248.10^\circ, 16.20^\circ \pm 73.80^\circ)$ given by the JLA in the Finslerian cosmological model. The angular difference between the two dipole directions is only 10.44°. We also found that the dipole direction given by the X-ray and UV fluxes of quasars is not far away from the dipole directions given by SNe Ia in the dipole-modulated

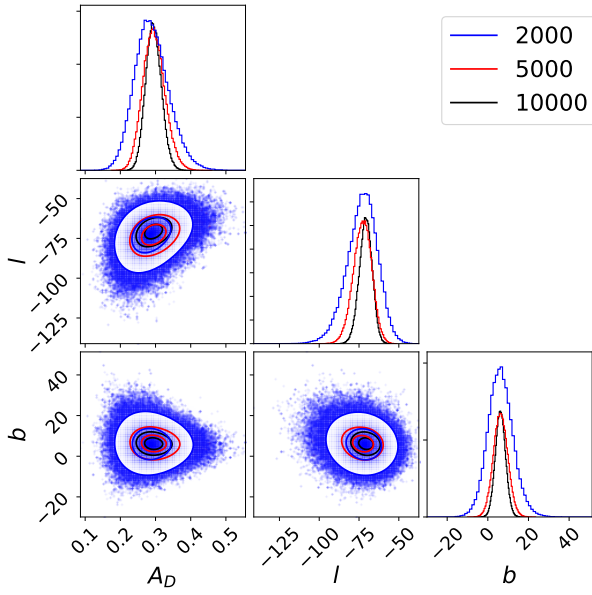


Figure 7. The marginalized posterior distribution of the parameters of dipole with the simulated X-ray and UV fluxes of quasars. The horizontal and vertical solid black lines denote the maximum of 1-dimensional marginalized posteriors. The blue, red, dark lines denote 2000, 5000 and, 10000 simulations, respectively.

Λ CDM model and the angular difference is around 30° . We thought the dipole direction from the X-ray and UV fluxes of quasars close to the ones from the SNe Ia sample, especially the JLA compilation, may hint that there could exist an underlying relation. We combined the Pantheon sample and JLA compilation with quasars to constrain the Finslerian cosmological model and the results are similar to the ones given by the Pantheon sample in the Finslerian cosmological model [51]. We also investigated the Hubble constant H_0 in the Finslerian cosmological model by combining the X-ray and UV fluxes of quasars with six gravitationally lensed quasars. We found a slightly smaller value of Hubble constant $H_0 = 72.2^{+3.6}_{-4.1} \text{ km s}^{-1} \text{ Mpc}^{-1}$ than the value $H_0 = 73.3^{+1.7}_{-1.8} \text{ km s}^{-1} \text{ Mpc}^{-1}$ given by the six gravitationally lensed quasars. At last, we forecasted the future constraints on the dipole parameters with the X-ray and UV fluxes of quasars. We constructed 2000, 5000, and 10000 simulations and found that the precisions of the parameters related to anisotropy have a significant improvement as the number of simulations increases. Our results show that the X-ray and UV fluxes of quasars have a promising future as a probe of anisotropy in the Finsler spacetime.

Acknowledgments

We thank Yong Zhou for helpful discussions. J.-Q.Xia is supported by the National Science Foundation of China under grants No. U1931202, 11633001, and 11690023; the

National Key R&D Program of China No. 2017YFA0402600.

References

1. G. Hinshaw *et al.*, *Astrophys. J. Suppl.* **208**, 19 (2013).
2. C. L. Bennett *et al.*, *Astrophys. J. Suppl.* **208**, 20 (2013).
3. N. Aghanim *et al.*, *Astron. Astrophys.* **641**, A1 (2020).
4. N. Aghanim *et al.*, *Astron. Astrophys.* **641**, A5 (2020).
5. N. Aghanim *et al.*, *Astron. Astrophys.* **641**, A6 (2020).
6. Y. Akrami *et al.*, *Astron. Astrophys.* **641**, A7 (2020).
7. M. Tegmark, A. de Oliveira-Costa, and A. Hamilton, *Phys. Rev. D* **68**, 123523 (2003).
8. P. Bielewicz, K. M. Gorski, and A. J. Banday, *Mon. Not. Roy. Astron. Soc.* **355**, 1283 (2004).
9. C. J. Copi, D. Huterer, D. J. Schwarz, and G. D. Starkman, *Mon. Not. Roy. Astron. Soc.* **449**, 3458 (2015).
10. Z. Chang, X. Li, and S. Wang, *Chin. Phys. C* **39**, 055101 (2015).
11. J. Kim and P. Naselsky, *Phys. Rev. D* **82**, 063002 (2010).
12. J. Kim and P. Naselsky, *Astrophys. J. Lett.* **714**, L265 (2010).
13. A. Gruppiso *et al.*, *Mon. Not. Roy. Astron. Soc.* **411**, 1445 (2011).
14. H. Liu, A. M. Frejsel, and P. Naselsky, *JCAP* **07**, 032 (2013).
15. W. Zhao, *Phys. Rev. D* **89**, 023010 (2014).
16. H. K. Eriksen *et al.*, *Astrophys. J.* **605**, 14 (2004), [Erratum: *Astrophys. J.* 609, 1198 (2004)].
17. F. K. Hansen, A. J. Banday, and K. M. Gorski, *Mon. Not. Roy. Astron. Soc.* **354**, 641 (2004).
18. H. K. Eriksen *et al.*, *Astrophys. J. Lett.* **660**, L81 (2007).
19. J. K. Webb *et al.*, *Phys. Rev. Lett.* **107**, 191101 (2011).
20. J. A. King *et al.*, *Mon. Not. Roy. Astron. Soc.* **422**, 3370 (2012).
21. C. Bonvin, R. Durrer, and M. Kunz, *Phys. Rev. Lett.* **96**, 191302 (2006).
22. R.-G. Cai, Y.-Z. Ma, B. Tang, and Z.-L. Tuo, *Phys. Rev. D* **87**, 123522 (2013).
23. T. Koivisto and D. F. Mota, *JCAP* **06**, 018 (2008).
24. Z. Chang, X. Li, H.-N. Lin, and S. Wang, *Eur. Phys. J. C* **74**, 2821 (2014).
25. Z. Chang and H.-N. Lin, *Mon. Not. Roy. Astron. Soc.* **446**, 2952 (2015).
26. H.-N. Lin, X. Li, and Z. Chang, *Mon. Not. Roy. Astron. Soc.* **460**, 617 (2016).
27. D. Hutsemekers, R. Cabanac, H. Lamy, and D. Sluse, *Astron. Astrophys.* **441**, 915 (2005).
28. Y. Zhou, Z.-C. Zhao, and Z. Chang, *Astrophys. J.* **847**, 86 (2017).
29. Z. Chang, H.-N. Lin, Z.-C. Zhao, and Y. Zhou, *Chin. Phys. C* **42**, 115103 (2018).
30. Z. Chang and Y. Zhou, *Mon. Not. Roy. Astron. Soc.* **486**, 1658 (2019).
31. J. A. Baldwin, *Astrophys. J.* **214**, 679 (1977).
32. D. Watson, K. D. Denney, M. Vestergaard, and T. M. Davis, *Astrophys. J. Lett.* **740**, L49 (2011).
33. F. Melia, *JCAP* **01**, 027 (2014).
34. E. Kilerci Eser *et al.*, *The Astrophysical Journal* **801**, 8 (2015).
35. J. M. Wang *et al.*, *Phys. Rev. Lett.* **110**, 081301 (2013).
36. F. La Franca *et al.*, *Astrophys. J. Lett.* **787**, L12 (2014).

37. G. Risaliti and E. Lusso, *Astrophys. J.* **815**, 33 (2015).
38. N. Khadka and B. Ratra, *Mon. Not. Roy. Astron. Soc.* **492**, 4456 (2020).
39. N. Khadka and B. Ratra, (2020).
40. E. Lusso *et al.*, *Astron. Astrophys.* **642**, A150 (2020).
41. H. Tananbaum *et al.*, *Astrophys. J.* **234**, L9 (1979).
42. G. Zamorani *et al.*, *Astrophys. J.* **245**, 357 (1981).
43. Y. Avni and H. Tananbaum, *Astrophys. J.* **305**, 83 (1986).
44. D. M. Scolnic *et al.*, *Astrophys. J.* **859**, 101 (2018).
45. M. Betoule *et al.*, *Astron. Astrophys.* **568**, A22 (2014).
46. K. C. Wong *et al.*, *Mon. Not. Roy. Astron. Soc.* **498**, 1420 (2020).
47. S. Refsdal, *Mon. Not. Roy. Astron. Soc.* **128**, 307 (1964).
48. D. Zhao, Y. Zhou, and Z. Chang, *Mon. Not. Roy. Astron. Soc.* **486**, 5679 (2019).
49. Z. Chang, H.-N. Lin, Y. Sang, and S. Wang, *Mon. Not. Roy. Astron. Soc.* **478**, 3633 (2018).
50. H.-N. Lin, S. Wang, Z. Chang, and X. Li, *Mon. Not. Roy. Astron. Soc.* **456**, 1881 (2016).
51. Z. Chang, D. Zhao, and Y. Zhou, *Chin. Phys. C* **43**, 125102 (2019).
52. Z. Chang *et al.*, *Mon. Not. Roy. Astron. Soc.* **479**, 1327 (2018).
53. X. Li, H.-N. Lin, S. Wang, and Z. Chang, *Eur. Phys. J. C* **75**, 181 (2015).
54. D. Foreman-Mackey, D. W. Hogg, D. Lang, and J. Goodman, *Publ. Astron. Soc. Pac.* **125**, 306 (2013).
55. X. Yang, F. Y. Wang, and Z. Chu, *Mon. Not. Roy. Astron. Soc.* **437**, 1840 (2014).